

Liquid-Liquid Two-Phase Flow Patterns in a Rectangular Microchannel

Yuchao Zhao

Dalian Institute of Chemical Physics, Chinese Academy of Sciences, Dalian 116023, Liaoning, China; and Graduate Univ., Chinese Academy of Sciences, Beijing 100049, China

Guangwen Chen and Quan Yuan

Dalian Institute of Chemical Physics, Chinese Academy of Sciences, Dalian 116023, Liaoning, China

DOI 10.1002/aic.11029

Published online October 30, 2006 in Wiley InterScience (www.interscience.wiley.com).

In this work, the flow of immiscible fluids in a PMMA microchannel 300 μm wide and 600 μm deep was investigated experimentally. Dyed de-ionized water and kerosene were selected as the test fluids. Flow patterns were observed by using a CCD camera and were identified by examining the video images. Flow patterns obtained at the T-junction and in the microchannel are presented. Superficial velocities varied between $9.26 \times 10^{-4} \sim 1.85$ m/s for water and $9.26 \times 10^{-4} \sim 2.78$ m/s for kerosene. The formation mechanism of slug, monodispersed droplet and droplet populations at the T-junction was studied. Weber numbers of water and kerosene, We_{KS} and We_{WS} , were used to predict the flow regime transition and the flow patterns map. The experimental data of volume of dispersed phase were successfully correlated as a function of We_{KS} , We_{WS} , and hold-up fraction. Considering the uncertainty associated with experimental quantification of the process, the results are in satisfactory agreement over the wide range of $1.90 \times 10^{-3} < We_{WS} < 30.43$ and $5.90 \times 10^{-6} < We_{KS} < 0.13$ with average absolute deviation of only 16.18%. © 2006 American Institute of Chemical Engineers AIChE J, 52: 4052–4060, 2006

Keywords: microchannel, microreactor, flow pattern, slug flow, two-phase flow

Introduction

Within the last decade, microchannel reactors have become a new and promising technology in chemistry, chemical engineering, and biotechnology.^{1–4} Processes based on multiphase reactions in microchemical systems, especially liquid-liquid two-phase reactions, occur in a broad range of application areas, such as nitration,⁵ extraction,⁶ emulsification,⁷ and so forth, and can form the basis for manufacture of a large variety of intermediate and consumer end-products. In spite of its technological importance, the details of the transfer processes

for liquid-liquid two phases in microsystems are not very well understood, especially those involving heterogeneous reactions where mass transfer and chemical reaction compete between themselves in a way. In fact, it was shown that scaling down the typical length scale could greatly increase mass and heat transfer efficiency and minimize amount of fluids, thus eventually resulting in shorter reaction times and reducing the cost of research and development. For the optimization of the design and the operation of two-phase flow systems, especially mass transfer, chemical reaction, and pressure drop in the microchannel, there was a need for researchers to predict accurately the existing flow patterns. A great number of studies have been carried out to understand gas-liquid two-phase flow regimes in the microchannels^{8–12}; however, not much was known regarding the simultaneous

Correspondence concerning this article should be addressed to G. W. Chen at gwchen@dicp.ac.cn.

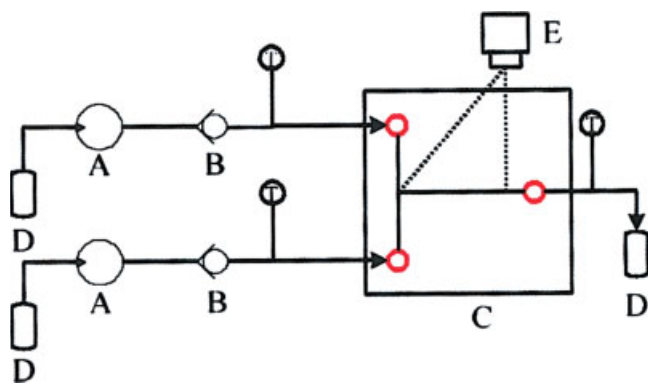


Figure 1. Schematic diagram of experimental setup. A: pump; B: check valve; C: T-shaped microchannel; D: tank; E: CCD camera.

[Color figure can be viewed in the online issue, which is available at www.interscience.wiley.com.]

flow of two immiscible liquids.¹³ There was no guarantee that the information available for gas-liquid cases could be extrapolated to liquid-liquid flows, and little attention had even been paid to the immiscible liquid-liquid two-phase flow patterns in microchannels.

Early studies of the immiscible liquid-liquid two-phase flow patterns predominantly consisted of flow in circular tubes with diameter $D_H > 10$ mm. Nadler and Mewes,¹⁴ Brauner and Maron,¹⁵ and Angeli and Hewitt¹⁶ experimentally investigated oil-water two-phase flow in a horizontal straight pipe and clarified flow regimes as stratified, stratified-dispersed, annular, slug, dispersed, and so forth. Although some flow regimes associated with liquid-liquid two-phase flow in large pipes, such as slug,¹⁷ also occurred in microchannels, some important differences existed between flow patterns in the two kinds of systems.

Recently, the flow of immiscible fluids in microchannels has attracted significant attention. The interest on flow patterns arose because the microfluidic technology could offer new prospects for emulsion science¹⁸; on the other hand, the progress of microchemical engineering required us to know the flow patterns in microchannels.¹ If the two fluids are miscible, parallel streams are able to flow side by side at low Reynolds number and diffuse freely from one stream to the other in microchannels. If the two fluids are immiscible fluids, the interfacial tension dominates on the effect of the dynamics of the free surface.¹⁹ Shearing by interfacial tension is advantageous to a micrometer scale because the effects of interfacial tension are significantly greater than gravitational force; this can be proved by the following dimensionless number, Bond number:

$$Bo = \frac{\text{Gravitational force}}{\text{Interfacial tension}} = \frac{\rho g D_H^2}{\sigma} \quad (1)$$

Obviously, the interfacial tension plays an important role in microfluidic flows when the characteristic length is small. With these ideas in mind, Hudson et al.^{20,21} developed a microfluidic approach to rapidly measure interfacial tension σ of immiscible fluids. Thorsen et al.²² demonstrated that microfluidic devices could be used to create controllable

droplet emulsions in immiscible fluids, by injection of water into a stream of oil at a T-junction. Guillot and Colin²³ had determined the stability of parallel flows in a microchannel after a T-junction with confocal fluorescence microscopy and identified three typical flow patterns, namely, droplets formed at the T-junction, parallel flows, and parallel flows that break into droplets inside the channel. On the other hand, the liquid-liquid slug flow capillary microreactor had been shown to be a useful technique for the elucidation and enhancement of reaction rate, which was limited by heat and mass transfer.^{17,24,25}

The objective of this article is to experimentally study the immiscible liquid-liquid two-phase flow patterns in T-junction rectangular microchannels with a hydraulic diameter of 0.4 mm. Dyed de-ionized water and kerosene are used as the working fluids. Flow patterns are observed by using a CCD camera and are identified by examining the video images.

Experimental

A schematic diagram of the experimental apparatus is shown in Figure 1. The working fluids are kerosene and de-ionized water with minute amounts of methylene blue dissolved in it for better visualization of the flow phenomena. The de-ionized water is first boiled in a beaker to remove the dissolved gases and fully degassed. Water and kerosene are forced to flow through the horizontal rectangular microchannel by high precision piston pumps (Beijing Satellite Manufacturing Factory). The physical properties of water and kerosene are listed in Table 1.

Our microchannel was fabricated in the PMMA plate using micromachining technology, and its surface was modified by sodium hydroxide for increasing hydrophilic property. The cross section is $300 \mu\text{m} \times 600 \mu\text{m}$, and its length is 60 mm. This results in hydraulic diameter D_H :

$$D_H = \frac{4A}{2H + 2W} = 400 \mu\text{m} \quad (2)$$

The microdevice has two inlet arms that meet at a T-junction. The flow patterns are observed at the T-junction and in the main channel after the T-junction. The essential features of the micro T-microchannel are shown in Figure 2.

The 3-D profile of the channel shown in Figure 2b is examined by using the Super Depth Surface Profile Measurement Microscope (VK-8550). The maximum and minimum values for depth and width are about $308 \mu\text{m}$ and $295 \mu\text{m}$, and $598 \mu\text{m}$ and $602 \mu\text{m}$, respectively.

The flow patterns are identified using a digital video camera that is connected to a personal computer and provides snapshots. A high-speed camera system (UC-610CL) with recording speed of 61 frames per second and shutter speed of

Table 1. Physical Properties of Water and Kerosene (at 293K and atmospheric pressure)

Fluid	Density	Viscosity
	kg/m ³	Pa·s
Water	998.2	0.001
Kerosene	780	0.00115

Interfacial tension σ 0.045 N/m.

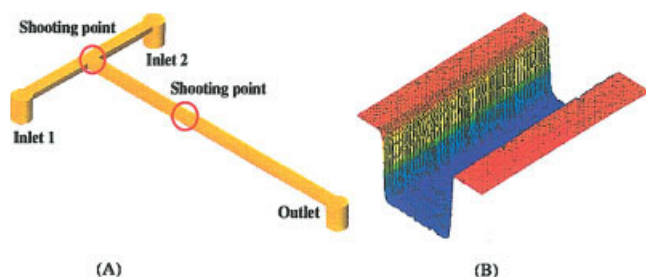


Figure 2. (a) Schematic of the T-junction rectangular microchannel; (b) 3-D profile of the microchannel.

[Color figure can be viewed in the online issue, which is available at www.interscience.wiley.com.]

1/110 ~ 1/110,000 sec was mounted together with a microscope. To observe distinctly the structure of the liquid-liquid flow patterns inside the microchannel, the extension tube is used to regulate the magnified multiple of the video camera. The light beam used for the visualization is provided through an adjustable light source under the test section.

It has been confirmed that liquid-liquid two-phase flow structures in microchannels are more seriously affected by the wettability between the wall and the fluids. So, for obtaining the oil droplets in the microchannel, we must make surface modifications to increase the surface wettability of the PMMA chip. The surface modification procedure was as follows. First, the test PMMA chip was cleaned with a soft brush, then it was washed in de-ionized water and pure ethanol for 2~3 min by ultrasonic vibration. Second, the chip was blown by filtered air and placed in sodium hydroxide (10 wt%) at 80°C for 2~3 h, then was washed in de-ionized water for 2~3 min. Finally, the test microchannel PMMA chip was blown by filtered air and installed to the experimental apparatus for measurements.

Results and Discussion

All experiments in the rectangular microchannel are conducted at room temperature and atmospheric pressure. The kerosene and water superficial velocity can be calculated by the following equations:

$$U_{KS} = \frac{Q_K}{A} \quad (3)$$

$$U_{WS} = \frac{Q_W}{A} \quad (4)$$

In our experiments, the ranges of water and kerosene superficial velocities are $9.26 \times 10^{-4} \sim 1.85$ m/s and $9.26 \times 10^{-4} \sim 2.78$ m/s, respectively. All runs were carried out at the constant ratio of water and kerosene by increasing the volumetric flux of kerosene and water simultaneously. Every run must be repeated no less than twice to ensure the reproducibility of snapshots.

Flow patterns at the T-junction

In this section, a comprehensive study of immiscible fluids flow and the formation processes of flow patterns at the T-

junction were performed. For illustrating the formation processes of flow patterns at the T-junction, the shooting points were chosen elaborately and shown in Figure 2a. In our experiments, using water and kerosene as work fluids, depending on the flow rates applied to each liquid inlet stream, six distinct flow patterns were observed based on visual observation of a video tape replay (61frames/s) and are shown in Figure 3.

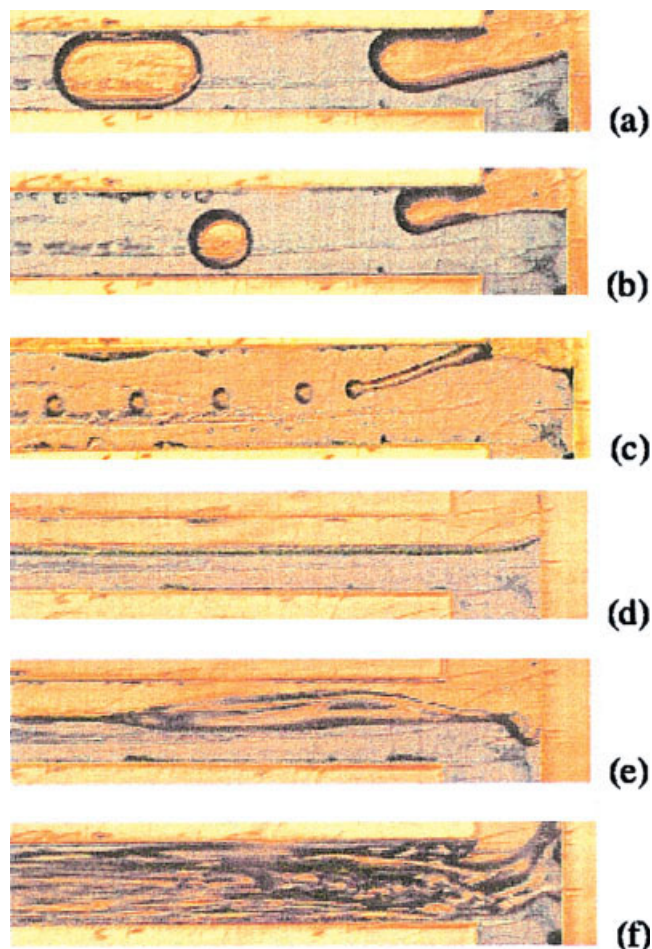


Figure 3. Flow patterns at the T-junction. (a) Oil slugs formed at the T-junction (ST), $q = 20$, $We_{KS} = 5.94 \times 10^{-6}$, $We_{WS} = 3.04 \times 10^{-3}$; (b) Mono-dispersed droplets formed at the T-junction (MDT), $q = 20$, $We_{KS} = 5.94 \times 10^{-4}$, $We_{WS} = 3.04 \times 10^{-1}$; (c) Drop populations formed in the center of the microchannel (DPM), $q = 40$, $We_{KS} = 1.34 \times 10^{-1}$, $We_{WS} = 2.74$; (d) Parallel flows that have smooth interface formed at the T-junction (PFST), $q = 1$, $We_{KS} = 5.35 \times 10^{-1}$, $We_{WS} = 6.85 \times 10^{-1}$; (e) Parallel flows that have wavy interface formed at the T-junction (PFWT), $q = 1$, $We_{KS} = 5.94$, $We_{WS} = 7.61$; (f) Chaotic thin striations flow formed at the T-junction (CTST), $q = 0.5$, $We_{KS} = 53.50$, $We_{WS} = 17.12$.

[Color figure can be viewed in the online issue, which is available at www.interscience.wiley.com.]

Surface effects become dominant due to the small size of microsystem devices. In fact, interfacial tension and inertial force are competing stresses that could distort the interface in this particular device. The interfacial tension tends to reduce the interfacial area, while inertia force is inclined to extend and drag the interface downstream. In order to determine the relative importance of inertia force and interfacial tension for the formation of flow patterns, the Weber (We) number is calculated. The Weber number yields the ratio of inertia force to interfacial tension. Since the Weber number includes the phase velocity term, in the absence of actual phase velocity measurements, the Weber numbers of water and kerosene are calculated in terms of the superficial velocities, as follows:

$$We_{WS} = \frac{D_H \cdot U_{WS}^2 \cdot \rho_W}{\sigma} \quad (5)$$

$$We_{KS} = \frac{D_H \cdot U_{KS}^2 \cdot \rho_K}{\sigma} \quad (6)$$

Within the range of flow rates and viscosity in our experiments, the Weber number covers a wide range of values, $5.94 \times 10^{-6} < We_{KS} < 53.5$ and $7.61 \times 10^{-6} < We_{WS} < 30.43$, and suggests a crossover from regimes dominated by interfacial tension to those dominated by inertia force.

Figure 3 shows that slug flow at the T-junction (ST) will appear when $7.61 \times 10^{-6} < We_{WS} < 4.87 \times 10^{-2}$ and $5.94 \times 10^{-6} < We_{KS} < 5.94 \times 10^{-4}$; in fact, these values suggest that interfacial tension dominates compared to inertial force, where q denotes the volumetric flux ratio (Q_W/Q_K). For given fixed oil flow rate Q_K , an increase in the rate of water results in the formation of monodispersed droplet (MDT). That is, under the constant value of We_{KS} , monodispersed droplets at the T-junction (MDT) begin to be formed with increasing We_{WS} , in the region of $7.6 \times 10^{-2} < We_{WS} < 0.78$ and $2.38 \times 10^{-5} < We_{KS} < 5.94 \times 10^{-4}$.

When $3.04 \times 10^{-3} < We_{WS} < 3.73$ and $2.38 \times 10^{-3} < We_{KS} < 1.49$, the parallel flow with smooth interface forms at the T-junction (PFST). As we increase the flow rates of water and oil, the We_{WS} and We_{KS} increase ($4.87 \times 10^{-2} < We_{WS} < 19.47$ and $2.38 \times 10^{-1} < We_{KS} < 10.05$), and the parallel flow with smooth interface turns to the parallel flow with wavy interface (PFWT), that is, the vortices are formed at the interface of two phases. Although the flow patterns that formed at the T-junction are different, the flow patterns may be developed into the same at the downstream due to the undeveloped flow at the T-junction. The two fluids collide at the T-junction and the vortices can be formed at the interface of two phases, but the energy of these vortices can be consumed in the downstream, and eventually results in vanishing of these vortices.

When $1.07 < We_{WS} < 30.43$ and $3.8 \times 10^{-4} < We_{KS} < 2.38 \times 10^{-1}$, the oil phase penetrates into the water phase as a jet, and droplet populations (DPM) are formed in the center of the microchannel. In this flow pattern, the water inertial effects dominate the system against the interfacial tension. This phenomenon is consistent with the classical Rayleigh-Plateau instability. The stream of kerosene flows between streams of water and is geometrically focused into a narrow cylindrical jet in the center of the microchannel at the T-

junction; the jet is destabilized by the Rayleigh-Plateau instability and forms droplet populations.

When $0.17 < We_{WS} < 30.43$ and $4.29 < We_{KS} < 53.5$, the chaotic thin striations flow are formed at the T-junction (CTST). In fact, this flow evolves eventually to annular flow at the downstream. The flow tends to instability because engulfment flow occurs at the T-junction²⁶ under the conditions of increasing of flow rates of water and oil.

Figure 4 shows the formation mechanism of slug (oil) flow at the T-junction (ST). These oil slugs are formed by interfacial instability taking place at the T-junction. The formation of oil slugs relaxes the stress by decreasing the interfacial area. The oil and water phases form an interface at the T-junction. The pressure drop along the axis of the microchannel forces the tip of the oil stream into downstream. The tip advances in the microchannel by expanding in size and stops growing when it hits the channel walls. The oil acts as a plug blocking the water. This produces the formation of oil slugs, and the volume of the oil slugs decreases by increasing the superficial velocities of water and kerosene. Under our experimental conditions ($H < W$), it leads to the bulleted cylindrical slice-like oil slugs being then in contact with the top and bottom walls.

For a given fixed oil flow rate Q_K , an increase in the rate of the water results in the formation of monodispersed droplet (MDT). Figure 5 shows the process of the formation of monodispersed droplets. In this flow pattern, these low values of We affirm that interfacial tension overwhelms inertia force. But the values of We_{WS} show that the water phase inertial effects begin to play a significant role in forming monodispersed droplets. Due to $H < W$, monodispersed droplets are squeezed between the top and bottom wall, and have a disc-like geometry.

Flow patterns map at the T-junction

Figure 6 shows a flow pattern map obtained for kerosene-water two-phase flow at the T-junction. The ordinate and abscissa were the Weber numbers of kerosene and water phase,

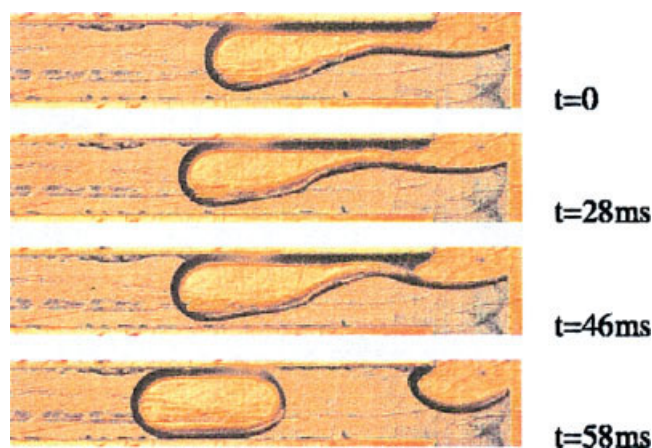


Figure 4. Oil slugs formation mechanism at the T-junction, $q = 10$, $We_{KS} = 2.38 \times 10^{-5}$, $We_{WS} = 3.04 \times 10^{-3}$.

[Color figure can be viewed in the online issue, which is available at www.interscience.wiley.com.]

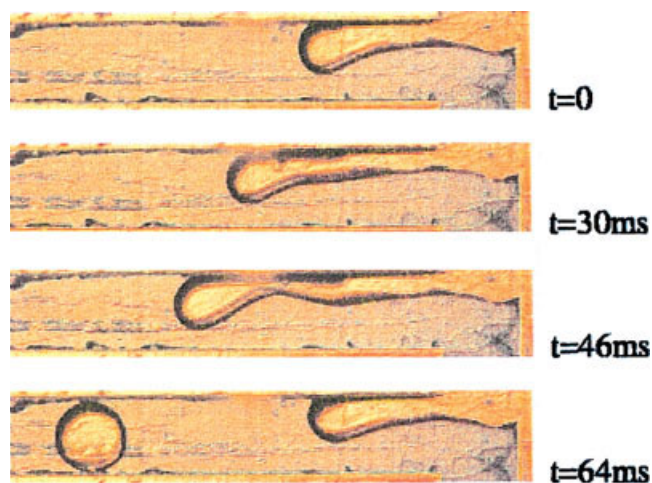


Figure 5. Monodispersed droplets formation mechanism at the T-junction, $q = 25$, $We_{KS} = 1.48 \times 10^{-4}$, $We_{WS} = 0.12$.

[Color figure can be viewed in the online issue, which is available at www.interscience.wiley.com.]

respectively. In liquid-liquid flow, some of the flow regimes were very similar to those encountered in gas-liquid flow. The Weber number transition model was suggested by Zhao and Rezkallah²⁷ and later modified by Rezkallah²⁸ and Akbar and coworkers²⁹ to provide a dimensionless flow regime map based on the Weber number estimated from the liquid and gas velocities. Furthermore, they argued that the entire flow patterns map could be divided into three regions: the interfacial tension dominated zone where interfacial tension effect predominates inertia force, the inertia dominated zone where inertia force was significantly larger than the interfacial tension, and the transition zone where inertia force and interfacial tension were comparable. In accordance with the above discussion, we divided the flow patterns map into the three regions shown in Figure 6:

(a) Zone I: the interfacial tension dominated, including ST, MDT, and PFST, for $(We_{KS} < 1) \cap (We_{WS} < 1)$;

(b) Zone II: the inertia and interfacial tension were comparable, including PFWT and DPM, for $[(We_{KS} < 10) \cap (We_{WS} < 10)] \cap [(We_{WS} > 1) \cup (We_{KS} > 1)]$;

(c) Zone III: the inertia dominated, including DPM and CTST, for $(We_{KS} > 10) \cup (We_{WS} > 10)$.

Flow patterns in the microchannel

For obtaining flow patterns in the fully developed flow in the microchannel, the condition of high L/D_H ratio must be satisfied for minimizing the entrance and exit effects. In our experiments, the distance from the shooting point to the entrance or exit was 30 mm, so the L/D_H ratio could reach 75. Unlike in large channels, the stratified flow could not be observed in our rectangular microchannel, and the parallel flow pattern became more prevalent. Figure 7 displays representative photographs of the identified fully developed flow patterns in the rectangular microchannel. In liquid-liquid flow in microchannels, some of the flow patterns are very

similar to those encountered in gas-liquid flow, but there are some important differences, such as no parallel flow for gas-liquid and the shape of dispersed phase is more regular for liquid-liquid. Like the definition of gas-liquid two-phase flow patterns, the essential characteristics of these flow patterns could be described as follows.

Slug flow (Figure 7a): When the liquid-liquid two-phase Weber numbers are very low, the oil phase can form larger drops that its maximum length larger than microchannel width. From experimental observation it is quite clear that the slug flow is an entrance phenomenon rather than induced from the microchannel inside. This flow pattern often appears at large superficial flow ratio of water to oil and small total superficial flow rate, but a transition to parallel flow occurs as the water/oil ratio decreases. The surface tension force keeps the oil phase to a slug structure, and slug coalescence is also seldom observed in the present experiment. This flow pattern had been proved to be a useful flow regime for the elucidation and intensification of reaction processes limited by heat and mass transfer rate.^{17,24,25}

Monodispersed droplets flow (Figure 7b): The oil phase is dispersed, forming discrete drops in the continuous water phase. They have a disc-like geometry and the distance between two consecutive monodispersed droplets is much longer than the microchannel width. The occurrence of the monodispersed flow is also an entrance phenomenon.

Droplet populations flow (Figure 7c): In this pattern, a bunch of well-defined spherical droplets are formed. These droplets are produced by an interfacial instability and inertia of the water and kerosene in the microchannel. In this regime, the coalescence was not seen. The distance between two consecutive droplets is smaller than the microchannel

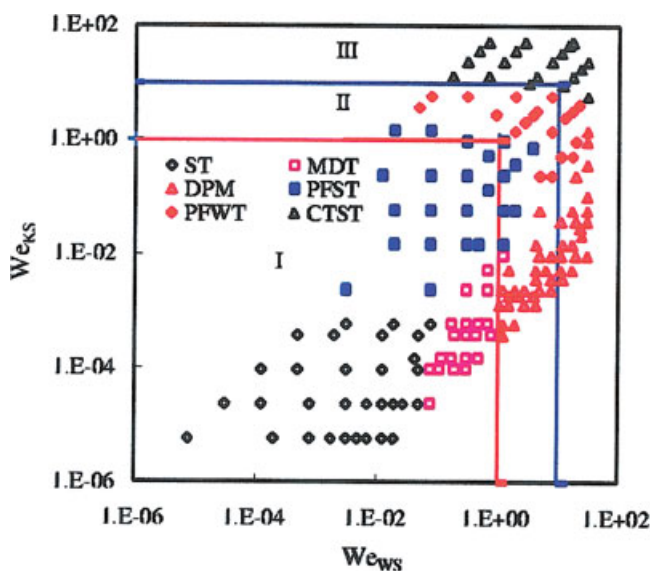


Figure 6. Flow patterns and flow pattern transition lines at the T-junction as a function of the kerosene superficial Weber number and the water superficial Weber number in a $300 \mu\text{m} \times 600 \mu\text{m}$ rectangular microchannel.

[Color figure can be viewed in the online issue, which is available at www.interscience.wiley.com.]

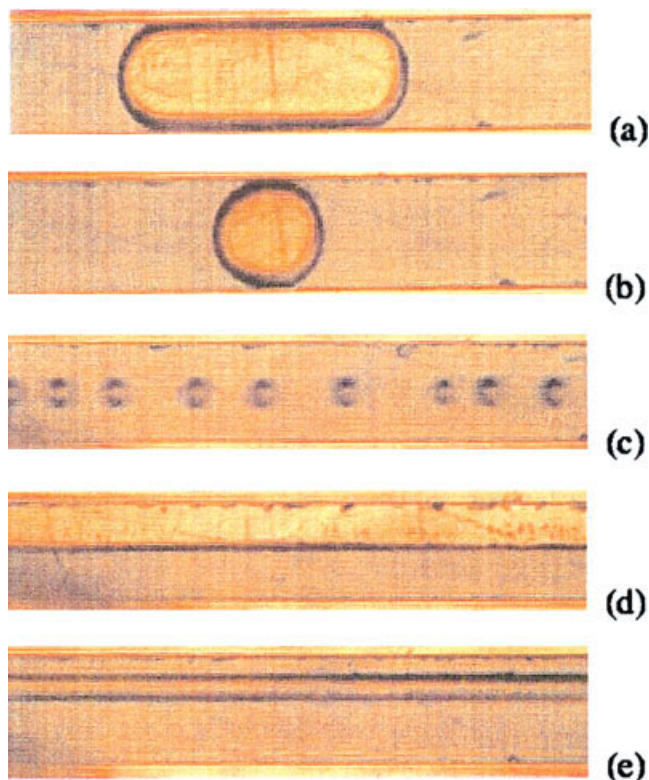


Figure 7. Representative photographs of stable flow patterns in the 0.4mm diameter rectangular microchannel. (a) Slug flow (SF), $q = 20$, $We_{KS} = 5.94 \times 10^{-6}$, $We_{WS} = 3.04 \times 10^{-3}$; (b) Monodispersed droplets flow (MDF), $q = 20$, $We_{KS} = 9.51 \times 10^{-5}$, $We_{WS} = 4.87 \times 10^{-2}$; (c) Droplets populations flow (DPF), $q = 10$, $We_{KS} = 5.94 \times 10^{-2}$, $We_{WS} = 7.61$; (d) Parallel flow (PF), $q = 1$, $We_{KS} = 13.37$, $We_{WS} = 17.12$; (e) Annular flow (AF), $q = 5$, $We_{KS} = 0.95$, $We_{WS} = 30.43$.

[Color figure can be viewed in the online issue, which is available at www.interscience.wiley.com.]

width. The forming of the drop populations flow is not an entrance phenomenon but rather induced from the microchannel inside.

Parallel flow (Figure 7d): The flow pattern corresponds to fluids flowing continuously side by side in the rectangular microchannel and is a way to perform solvent extraction or purification, which is a key operation in analytical processing.^{30,31} The interface of the two phases can be smooth or wavy at the T-junction; however, it eventually evolves into a smooth interface in the fully developed flow. When the water/kerosene ratio is greater than unity, the flow pattern tended to parallel flow. An increase in the total superficial velocity leads to annular flow.

Annular flow (Figure 7e): The characteristic of annular flow is the continuity of the oil phase in the water phase. The water phase flows near the walls of the microchannel. This flow pattern often appears at large total superficial velocity and evolves from chaotic thin striations flow that is formed at the T-junction.

Flow patterns map in the microchannel

The overall immiscible liquid-liquid two-phase flow pattern map under the condition of fully developed flow is shown in Figure 8. Compared to the flow patterns at the T-junction, five well-defined patterns are only observed at the fully developed flow in the microchannel. Like the flow patterns map at the T-junction, we divide the flow patterns map into three regions, as follows:

- (a) Zone I: interfacial tension dominated, including SF, MDF, and PF, for $(We_{KS} < 1) \cap (We_{WS} < 1)$;
- (b) Zone II: inertia and interfacial tension are comparable, including PF and DPF, for $[(We_{KS} < 10) \cap (We_{WS} < 10)] \cap [(We_{WS} > 1) \cup (We_{KS} > 1)]$;
- (c) Zone III: inertia dominated, including PF, DPF, and AF, for $(We_{KS} > 10) \cup (We_{WS} > 10)$.

Volume size of dispersed phase

In the chemical and food industries, liquid-liquid dispersions appear in processes, such as emulsification and two-phase reactions. The dispersed phase size will have implications for the heat and mass transfer rates and the design of downstream separation equipment. According to the above discussion, two factors determine the dispersed phase size in microchannels, inertia force and interfacial tension. So in the present work, we only are concerned with dispersed flow patterns, MDF, DPF, and SF. The volume of the oil phase (dispersed phase) is calculated from high-speed video pictures and plotted as a function of kerosene flow rate in a $300 \mu\text{m} \times 600 \mu\text{m}$ microchannel, and the results are demonstrated in Figure 9.

As expected, the volume of the dispersed phase decreases in all cases with increase of total flow rate. Furthermore, for

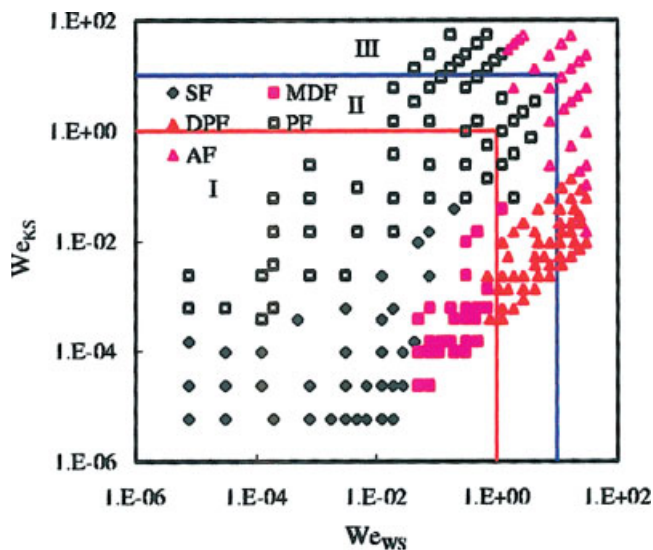


Figure 8. Flow patterns and flow pattern transition lines in the microchannel as a function of the kerosene superficial Weber number and the water superficial Weber number in a $300 \mu\text{m} \times 600 \mu\text{m}$ rectangular microchannel.

[Color figure can be viewed in the online issue, which is available at www.interscience.wiley.com.]

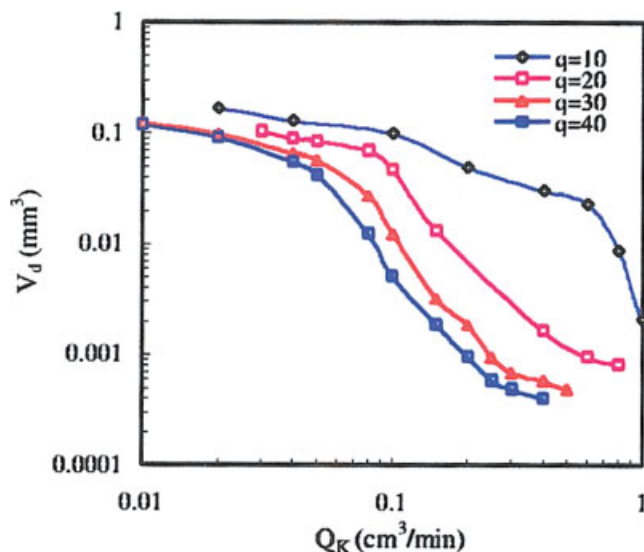


Figure 9. Evolution of the dispersed phase volumes (V_d) as a function of the kerosene flow rate in a $300\mu\text{m} \times 600\mu\text{m}$ microchannel.

[Color figure can be viewed in the online issue, which is available at www.interscience.wiley.com.]

a given kerosene flow rate, the volume of the dispersed phase decreases with increasing volumetric flux ratio q . This means on the other hand that for applications where an oil phase flow rate is given, an aimed volume of dispersed phase can be achieved by choosing the appropriate volumetric flux ratio. In fact, the smaller volume of dispersed phase corresponds to higher energy input, that is, the effect of inertia force becomes important. According to the above analysis, the volume of dispersed phase can

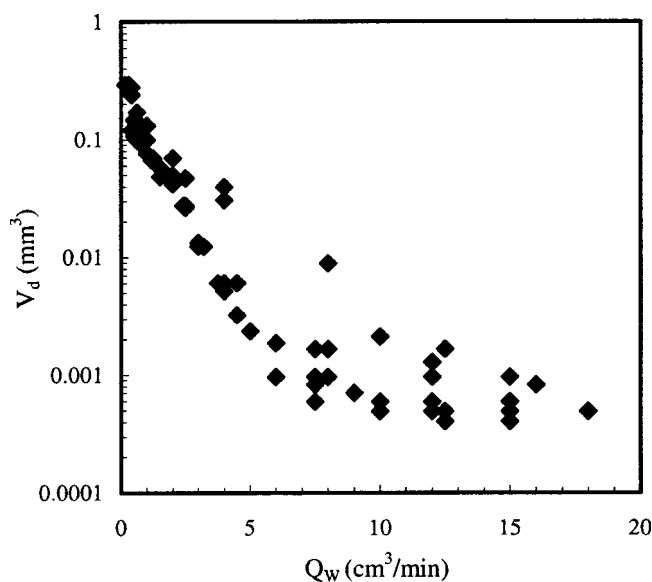


Figure 10. Effect of flow rate of the water phase on the volume of the dispersed phase.

depend on interfacial tension, inertia force, and the volumetric fraction of the dispersed phase. All the experimental results are plotted in Figure 10. By using the multi-variable least squares methods, the equivalent R can be correlated to superficial Weber number and the hold-up fraction as Eq. 3:

$$\frac{R}{D_H} = -0.1276 \ln \left[\frac{We_{WS} \cdot (1 - \varepsilon)}{(We_{KS} \cdot \varepsilon)^{0.15}} \right] + 0.5595 \quad (7)$$

where R and ε can be written as:

$$R = \sqrt[3]{\frac{3V_d}{4\pi}} \times 10^{-3} \quad (8)$$

$$\varepsilon = \frac{Q_K}{Q_K + Q_W} \quad (9)$$

The above correlation shows that the volume of the dispersed phase is more dependent on the water phase than the oil phase. The validity of using Eq. 7 to predict the experimental volume of the dispersed phase is shown in Figure 11. Absolute deviation is defined as:

$$\delta = \frac{|(V_d)_{cal} - (V_d)_{exp}|}{(V_d)_{exp}} \times 100\% \quad (10)$$

Considering the uncertainty associated with experimental quantification of the process, the results are in satisfactory agreement over the wide range of $1.90 \times 10^{-3} < We_{WS} < 30.43$ and $5.90 \times 10^{-6} < We_{KS} < 0.13$ with average absolute deviation of only 16.18%.

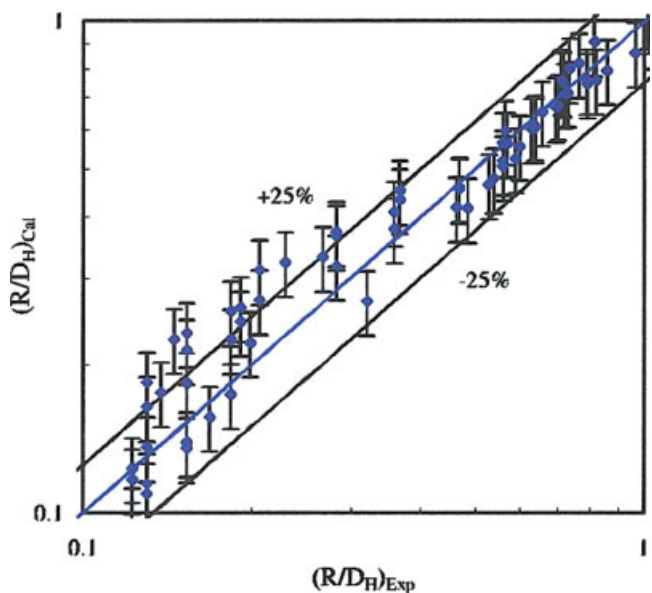


Figure 11. Comparison of experimental and calculated, from Eq. 7, volume of the dispersed phase in a $300\mu\text{m} \times 600\mu\text{m}$ rectangular microchannel.

[Color figure can be viewed in the online issue, which is available at www.interscience.wiley.com.]

Conclusions

Flow patterns and the process of formation mechanism of the dispersed phase with oil-water in a horizontal rectangular microchannel were studied in this article. The flow patterns map was correlated by interfacial tension and inertia force. The kerosene and water superficial velocities were varied in the $9.26 \times 10^{-4} \sim 2.78$ m/s and $9.26 \times 10^{-4} \sim 1.85$ m/s ranges, respectively.

Six distinct flow patterns can be identified at the T-junction: oil slugs formed at the T-junction, monodispersed droplets formed at the T-junction (MDT), droplet population formed in the center of the microchannel (DPM), parallel flows that have smooth interface at the T-junction (PFST), parallel flows that have wavy interface at the T-junction (PFWT), and chaotic thin striations flow formed at the T-junction (CTST). Three regions in the flow patterns map are divided into three zones, namely, interfacial tension dominated, inertial force and interfacial tension are comparable, and inertial force dominated. Five flow patterns are obtained in the microchannel, that is, monodispersed droplets flow, droplet population flow, slug flow, parallel flow, and annular flow. Liquid-liquid two-phase flow patterns transition maps at the T-junction and in the microchannel were constructed.

The volume of dispersed phase measurements is correlated to the superficial Weber number of water and kerosene, hold-up fraction. It is important to note that this study gives a contribution to the volume of dispersed phase quantification in liquid-liquid systems in T-shaped microchannels, which usually is not studied nor was possible to quantify in previous studies. This will serve as the basis for future mass transfer and reaction experimental work in multiphase microsystems.

Acknowledgments

We gratefully acknowledge financial support for this project from the National Natural Science Foundation of China and China National Petroleum Corporation (No. 20176057 and No. 20490208).

Notation

A = cross-sectional area of channel, m²
D_H = hydraulic diameter of microchannel, m
g = the gravitational constant, 9.81 m/s²
H = channel depth, m
L = channel length, m
q = Q_w/Q_k = volumetric flux ratio
Q = volumetric flow rate, m³/s
R = equivalent radius, m
U = superficial velocity, m/s
V_d = the volume of the dispersed phase, mm³
W = channel width, m
Re = Reynolds number
We = Weber number

Greek letters

ρ = mass density, kg/m³
σ = interfacial tension, N/m
ε = hold-up fraction
∩ = intersection
∪ = union

Subscripts

cal = calculated value
exp = experimental value
K = kerosene
S = superficial
W = water

Literature Cited

- Ehrfeld W, Hessel V, Löwe H. *Microreactor*. New York/Weinheim: Wiley/VCH; 2000.
- Jensen KF. Microreaction engineering—is small better? *Chem Eng Sci*. 2001;56:293–303.
- Jähnisch K, Hessel V, Löwe H, Baerns M. Chemistry in microstructured reactors. *Angew Chem Int Ed*. 2004;43:406–446.
- Chen GW, Yuan Q, Li HQ, Li SL. CO selective oxidation in a microchannel reactor for PEM fuel cell. *Chem Eng J*. 2004;101:101–106.
- Burns JR, Ramshaw C. A microreactor for the nitration of benzene and toluene. *Chem Eng Comm*. 2002;189:1611–1628.
- Tokeshi M, Minagawa T, Uchiyama K, Hibara A, Sato K, Hisamoto H, Kitamori T. Continuous-flow chemical processing on a microchip by combining microunit operations and a multiphase flow network. *Anal Chem*. 2002;74:1565–1571.
- Willaime H, Barbier V, Kloul L, Maine S, Tabeling P. Arnold tongues in a microfluidic drop emitter. *Phys Rev Lett*. 2006;96:054501.
- Triplett KA, Ghiaasiaan SM, Abdel-Khalik SI, Sadowski DL. Gas-liquid two-phase flow in microchannels, Part I: two-phase flow pattern. *Int J Multiphase Flow*. 1999a;25:377–394.
- Xu JL, Cheng P, Zhao TS. Gas-liquid two-phase flow regimes in rectangular channels with mini/microgaps. *Int J Multiphase Flow*. 1999;25:411–432.
- Mishima K, Hibiki T. Some characteristics of air-water two-phase flow in small diameter vertical tubes. *Int J Multiphase Flow*. 1996;22:703–712.
- Coleman JW, Garimella S. Characterization of two-phase flow patterns in small diameter round and rectangular tubes. *Int J Heat Mass Transfer*. 1999;42:2869–2881.
- Thulasidas TC, Abraham MA, Cerro RL. Bubble-train flow in capillaries of circular and square cross-section. *Chem Eng Sci*. 1995;50:183–199.
- Liu L, Matar OK, Lawrence CJ, Hewitt GF. Laser-induced fluorescence (LIF) studies of liquid-liquid flows. Part I: Flow structures and phase inversion. *Chem Eng Sci*. 2006;61:4007–4021.
- Nadler M, Mewes D. Flow induced emulsification in the flow of two immiscible liquids in horizontal pipes. *Int J Multiphase Flow*. 1997;23:55–68.
- Brauner N, Maron MD. Flow pattern transitions in two-phase liquid-liquid flow in horizontal tubes. *Int J Multiphase Flow*. 1992;18:123–140.
- Angeli P, Hewitt GF. Flow structure in horizontal oil-water flow. *Int J Multiphase Flow*. 2000;26:1117–1140.
- Burns JR, Ramshaw C. The intensification of rapid reactions in multiphase systems using slug flow in capillaries. *Lab on Chip*. 2001;1:10–15.
- Dreyfus R, Tabeling P, Willaime H. Ordered and disordered patterns in two-phase flows in microchannels. *Phys Rev Lett*. 2003;90:144505.
- Squires TM, Quake SR. Microfluidic: Fluid physics at the nanoliter scale. *Rev Mod Phys*. 2005;77:977–1026.
- Hudson SD, Goodrum WJ, Kathryn J, Beers L, Amis EJ. Microfluidic interfacial tensiometry. *Appl Phys Lett*. 2005;87:081905.
- Cabral JT, Hudson SD. Microfluidic approach for rapid multicomponent interfacial tensiometry. *Lab Chip*. 2006;6:427–436.
- Thorsen T, Roberts RW, Arnold FH, Quake SR. Dynamic pattern formation in a vesicle-generating microfluidic device. *Phys Rev Lett*. 2001;86:4163–4166.
- Guillot P, Colin A. Stability of parallel flows in a microchannel after a T junction. *Phys Rev E*. 2005;72:066301.
- Dummann G, Quittmann U, Groschel L, Agar DW, Worz O, Morgenschweis K. The capillary-microreactor: a new reactor concept for

- the intensification of heat and mass transfer in liquid-liquid reactions. *Catal Today*. 2003;79–80:433–439.
25. Kashid MN, Garlach I, Franzke J, Acker JF, Platte F, Agar DW, Turek S. Internal circulation within the liquid slugs of liquid-liquid slug flow capillary microreactor. *Ind Eng Chem Res*. 2005;44:5003–5010.
 26. Kockmann N, Föll C, Woias P. Flow regimes and mass transfer characteristics in static micro mixers. *Proc SPIE*. 2003;4982:319.
 27. Zhao L, Rezkallah KS. Gas-liquid flow patterns at microgravity conditions. *Int J Multiphase Flow*. 1993;19:751–763.
 28. Rezkallah KS. Weber number based flow-pattern maps for liquid-gas flows at microgravity. *Int J Multiphase Flow*. 1996;22:1265–1270.
 29. Akbar MK, Plummer DA, Ghiaasiaan SM. On gas-liquid two-phase flow regimes in microchannels. *Int J Multiphase Flow*. 2003;29:855–865.
 30. Hibara A, Nonaka M, Tokeshi M, Kitamori T. Spectroscopic analysis of liquid/liquid interfaces in multiphase microflows. *J Am Chem Soc*. 2003;125:14954–14955.
 31. Maruyama T, Matsushita H, Uchida JI, Kubota F, Kamiya N, Goto M. Liquid membrane operations in a microfluidic device for selective separation of metal ions. *Anal Chem*. 2004;76:4495–4500.

Manuscript received Jun. 15, 2006, revision received Sept. 4, 2006